*Egypt. J. Chem.* **Vol. 67**, No. 12 pp. 267 - 283 (2024)

**Egyptian Journal of Chemistry**

**http://ejchem.journals.ekb.eg/**

# Synthesis, Electronic Structure, NLO Analysis and Antitumor Activity of Some Novel Quinolinones Derivatives: DFT Approach

**Amal Gehad Salah[a]*, Shimaa Abdel Halim[a], Heba Hassan[a]**

*Department of Chemistry, Faculty of Education, Ain Shams University, Roxy 11711, Cairo, Egypt*

**Abstract**

In the present study, a novel series of 4-(2-benzylidenehydrazinyl)-1-ethylquinolin-2(1H)-one derivatives have been designed and synthesized from the reaction of 4-hydrazinoquinolin-2(1H)-one with 4-substituted benzaldehyde possessing electron donating and withdrawing groups. The structures of the obtained hydrazone compounds have been characterized in detail using IR, NMR, mass spectra and elemental analysis as well. The assigned chemical shifts of hydrazone compounds were compared with the NMR data. We observed that the presence of withdrawing group in hydrazonquinolinone showed a lower field than electron donating group. Also, the in vitro antitumor activity of all hydrazone compounds was investigated against human Hepatocellular carcinoma cell lines (HePG-2) using the colorimetric method and studying structure-activity relationship analysis (SARs). The electronic structures of some novel quinolinones derivatives are investigated using DFT/B3LYP/6-311++G (d, p) level of theory. In theoretical studies, the global chemical activity descriptors (FMOs, softness, hardness, electron affinity, ionization potential, etc.) and MEP were computed to predict important information related to the stability and reactivity of the prepared molecules. Compound 8 is the more stable product. To explain the nonlinear optical (NLO) properties of the synthesized compounds, the dipole moment, polarizability, and initial hyperpolarizability values (in the range 69 x 10-30 - 109 x 10-30 esu) have been calculated and compared with Para-Nitro-Aniline (PNA), as a reference material show promising optical properties. In addition, the 1H and 13C-NMR chemical shifts of the synthesized compounds were simulated by GIAO manner and compared with the experimental chemical shifts results.

***Keywords:*** Quinolinones Derivatives; DFT/ B3LYB/6-311++G (d,p); NLO; Antitumor Activity.

## 1.Introduction

Quinolinones have been considered a privileged scaffold in medicines for treating various diseases due to their biological and pharmacological activities [**1,2**], including antibiotics, antimicrobial [**3,4**], antimalarial [**5,6**], antibacterial [**7,8**], antifungal [**9**], antioxidant, anticancer [**10-12**] as anticancer drug applicants that strongly enhance cell apoptosis [**13**], antihistaminic or anti-inflammatory, antiallergic, antipsychotic [**14-16**], antidepressant, anticonvulsant [**17**], anti-viral [**18**], antiplatelet activities [**19-21**] , enzyme inhibitor [**22**]. Moreover, hydrazine and hydrazine derivatives, precisely heterocyclic-substituted hydrazine's, are well-known as useful synthons in organic chemistry [**23**]. Furthermore, many hydrazones and hydroxyquinoline derivatives show pharmacological activities, including antitumoral, antimicrobial, antimycobacterial, antimalarial, antiplatelet, antidepressant, anticonvulsant, analgesic and anti-inflammatory [**24-30**]. Density Functional Theory (DFT), is a method for calculating the electronic structures of atoms and molecules using the fundamental principles of quantum mechanics, furthermore, it is a method for illuminating the properties of the compounds [**31**]. In various fields, DFT represents a reliable and beneficial method to investigate the molecular structure, spectroscopic assignments of medicines/drugs [**32-34**], and risk assessment of chemicals [**35**]. Recently, in attention to the synthesis and biological importance of hydroxyquinoline derivatives and hydrazones, the present work deals with the design of hydrazones in quinolinone moiety to obtain new derivatives and study their anticancer activity as well as the structure-activity relationship [**36-39**]. There have not been any extensive theoretical or experimental studies on our novel synthesized quinolinone derivatives and their

*Corresponding author e-mail: amalgehad@edu.asu.edu.eg.; (Amal Gehad Salah).
EJCHEM use only: Received date 15 May 2024; revised date 23 June 2024; accepted date 02 July 2024
DOI: 10.21608/ejchem.2024.290027.9716

potential as a drug candidate is yet to be explored. Therefore, our study in this work is to explore the geometrical parameters (bond lengths, bond angles and dihedral angles), ground state properties of quinolinone derivatives, highest occupied molecular orbital (HOMO), lowest unoccupied molecular orbital (LUMO), energy gaps, the effect of substituents of different electron-donating and withdrawing strengths in the one aryl moiety, and electrostatic potential are calculated using B3LYP/6-311++G (d,p). The electronic dipole moment ($\mu$), and first order hyperpolarizability ($\beta$) values of the studied compounds have been calculated to study the NLO properties to identify and characterize the forces that govern the structure activity and the optical properties of the mentioned compounds. Finally, global reactivity descriptors including softness ($S$), hardness ($\eta$), electronegativity ($X$), electrophilicity ($\omega$), nucleophilicity ($\varepsilon$) and additional electronic charge ($\Delta N$) of the studied compounds were computed and analysed. As well, the electrostatic potential (ESP) and molecular electrostatic potential (MEP) of the synthesized molecules were explored. Moreover, obtaining confirmation of the experimental spectral data to corroborate the theoretical findings.

## 2. Experimental details

Melting points were determined on a Digital Stuart SMP-3 Melting Point Apparatus. IR spectra were recorded on a PerkinElmer FT-IR 1650 spectrophotometer; using samples in KBr disks, $^{1}$H-NMR (400 MHz) and $^{13}$C-NMR (100 MHz) spectra were recorded on Mercury 300BB or Gemini 300BB spectrometers (δ), using DMSO-d6 as solvents. Mass spectra (70 eV) were obtained using a Shimadzu GC-2010 gas chromatography instrument mass spectrometer. Elemental microanalyses were performed on a PerkinElmer CHN-2400 analyzer at Cairo University. (1-Ethyl-2-oxo-1,2-dihydro-4-quinolinyl) hydrazine (2) was synthesized according to literature method [**23**].

### *2.1. Synthesis and characterization of compounds*

#### *2.1.1. Preparation of compound **3-6***

A mixture of hydrazine **2** (2.03 g, 1 mmol) with different aldehydes; benzaldehyde, *P*-anisaldehyde, *P*-methylbenzaldehyde, *P*-hydroxybenzaldehyde (1 mmol) was refluxed for 15 min. in ethanol. The liquid mixture was left to cool at room temperature until complete precipitation occurred. Then, the solid precipitate was filtered off, dried, and recrystallized by ethanol to give hydrazone compounds.

4-(2-benzylidenehydrazinyl)-1-ethylquinolin-2(1*H*)-one (**3**)

Pale yellow, yield (2.47 g, 85 %), m.p= 281-283 °C; IR (KBr, cm$^{-1}$): 3223 (NH), 3082 (C-H$_{aromatic}$), 2983 (C-H$_{aliphatic}$), 1629 (C=O), 1605 (C=N), 1559 (C=C), 1447 (CH$_{2bending}$), 1396 (CH$_{3bending}$), 1130 (C-C), 967, 841, 753. $^{1}$H NMR (DMSO-$d_6$):$\delta_H$ =1.19 (t, 3H, $J$=8$_{Hz}$, CH$_3$), 4.23 (q, 2H, $J$=4 $_{Hz}$, CH$_2$), 6.39 (s, 1H, 3-CH), 7.28 (t, 1H, $J$=4 $_{Hz}$, 7-CH$_{quinolinone}$), 7.40 (m, 3H, *m,m,p*-CH$_{benzene}$), 7.56 (d, 1H, $J$=8 $_{Hz}$, 8-CH$_{quinolinone}$), 7.64 (t, 1H, $J$=8 $_{Hz}$, 6-CH$_{quinolinone}$), 7.77 (d, 2H, *o,o*-CH$_{benzene}$), 8.15 (d, 1H, $J$ =12 $_{Hz}$, 5-CH$_{quinolinone}$), 8.39 (s, 1H, N=CH), 10.80 (s, 1H, NH$_{disappeared\ with\ D2O}$ ). $^{13}$C NMR (DMSO-$d_6$):$\delta_C$ = 162, 148, 144, 139, 135, 132, 130, 129, 127, 127, 123, 123, 121, 115, 114, 95, 36, 13. MS (70 eV) : *m/z* (%) = 291 (M+) (95.23). Anal. Calcd for $C_{18}H_{17}N_3O$ (291.36) C 74.21; H 5.88; N 14.42 %. Found: C 74.18; H 5.82; N 14.36.

4-(2-(4-hydroxybenzylidene)hydrazinyl)-1-ethylquinolin-2(1*H*)-one (**4**)

Cumin, yield (2.46 g, 80 %), m.p = 302-304 °C decomp.; IR (KBr, cm$^{-1}$): 3300-2600 (OH$_{broad}$), 3296 (NH), 3046 (C-H$_{aromatic}$), 2991 (C-H$_{aliphatic}$), 1626 (C=O), 1600 (C=N), 1563 (C=C), 1465 (CH$_{2bending}$), 1401 (CH$_{3bending}$), 1130 (C-C), 975, 885, 765. $^{1}$H NMR (DMSO-$d_6$): $\delta_H$ = 1.18 (t, 3H, $J$=8 $_{Hz}$, CH$_3$), 4.22 (q, 2H, $J$=4 $_{Hz}$, CH$_2$), 6.33 (s, 1H, 3-CH ), 6.86 (d, 2H, *m,m*-CH$_{benzene}$), 7.26 (t, 1H, $J$=4 $_{Hz}$, 7-CH$_{quinolinone}$), 7.54 (d,1H, $J$=8 $_{Hz}$, 8-CH$_{quinolinone}$), 7.60 (m, 3H, *o,o*-CH$_{benzene}$,6-CH$_{quinolinone}$), 8.13 (d, 1H, $J$=8 $_{Hz}$, 5-CH$_{quinolinone}$), 8.30 (s, 1H, N=CH), 9.90 (s, 1H, OH$_{disappeared\ with\ D2O}$), 10.58 (s, 1H, NH$_{disappeared\ with\ D2O}$). $^{13}$C NMR (DMSO-$d_6$): $\delta_C$ = 162, 160, 148, 145, 139, 131, 131, 129, 126, 123, 121, 116, 116, 115, 114, 94, 36, 13. MS (70 eV) : *m/z* (%) = 307 (M+) (13.26). Anal. Calcd. For $C_{18}H_{17}N_3O_2$ (307.36) C 70.34; H 5.58; N 13.67. Found: C 70.23; H 5.55; N 13.63.

4-(2-(4-methylbenzylidene)hydrazinyl)-1-ethylquinolin-2(1*H*)-one (**5**)

Yellow, yield (2.44 g, 80 %), m.p = 282-284 °C; IR (KBr, cm$^{-1}$): 3260 (NH), 3099 (C-H$_{aromatic}$), 2972 (C-H$_{aliphatic}$), 1632 (C=O), 1601 (C=N), 1567 (C=C), 1445 (CH$_{2bending}$), 1397 (CH$_{3bending}$), 1131 (C-C), 952, 837, 778. $^{1}$H NMR (DMSO-$d_6$): $\delta_H$ = 1.19 (t, 3H, $J$=12 $_{Hz}$, CH$_3$), 2.34 (s, 3H, CH$_3$), 4.23 (q, 2H, $J$=8 $_{Hz}$, CH$_2$), 6.37 (s, 1H, 3-CH), 7.27 (m, 3H, *m,m*-CH$_{benzene}$,7-CH$_{quinolinone}$), 7.55 (d, 1H, $J$=8 $_{Hz}$, 8-CH$_{quinolinone}$), 7.63 (m, 3H, *o,o*-CH$_{benzene}$,6-CH$_{quinolinone}$), 8.14 (d, 1H, $J$=8 $_{Hz}$, 5-CH$_{quinolinone}$), 8.35 (s, 1H, N=CH), 10.75 (s, 1H, NH$_{disappeared\ with\ D2O}$). $^{13}$C NMR (DMSO-$d_6$): $\delta_C$ = 162, 148, 144, 140, 139, 133, 131, 130, 127, 127, 123, 123, 121, 115, 114, 95, 36, 22, 13. MS (70 eV) : *m/z* (%) = 305 (M+) (100.00). Anal. Calcd for $C_{19}H_{19}N_3O$ (305.38) C 74.73; H 6.27; N 13.76. Found: C 74.70; H 6.15; N 13.67.

4-(2-(4-methoxybenzylidene)hydrazinyl)-1-ethylquinolin-2(1*H*)-one (**6**)

Pale yellow, yield (2.41 g, 75 %), m.p = 245-247 °C; IR (KBr, $cm^{-1}$): 3278 (NH), 2968 (C-$H_{aromatic}$), 2930 (C-$H_{aliphatic}$), 1630 (C=O), 1605 (C=N), 1564 (C=C), 1453 ($CH_{2bending}$), 1362 ($CH_{3bending}$), 1133 (C-C), 961, 822, 749. $^1$H NMR (DMSO-$d_6$): $\delta_H$ = 1.18 (t, 3H, *J*=8 $_{Hz}$, $CH_3$), 3.81 (s, 3H, O-$CH_3$), 4.23 (q, 2H, *J*=8 $_{Hz}$, $CH_2$), 6.34 (s, 1H, 3-CH), 7.03 (d, 2H, *m,m*-$CH_{benzene}$), 7.27 (t, 1H, *J*=4 $_{Hz}$, 7-$CH_{quinolinone}$), 7.55 (d, 1H, *J*=8 $_{Hz}$, 8-$CH_{quinolinone}$), 7.64 (t, 1H, *J*=12 $_{Hz}$, 6-$CH_{quinolinone}$), 7.71 (d, 2H, *o,o*-$CH_{benzene}$), 8.13 (d,1H, *J*=8 $_{Hz}$, 5-$CH_{quinolinone}$), 8.33 (s, 1H, N=CH), 10.66 (s, 1H, $NH_{disappeared\ with\ D2O}$). $^{13}$C NMR (DMSO-$d_6$): $\delta_C$ = 162, 161, 148, 144, 139, 131, 131, 129, 128, 123, 121, 115, 115, 115, 114, 94, 56, 36, 13. MS (70 eV) : *m/z* (%) = 321 (100.00) (M+). Anal. Calcd for $C_{19}H_{19}N_3O_2$ (321.38) C 71.01; H 5.96; N 13.07. Found: C 70.87; H 5.89; N 13.04.

*2.1.2. Preparation of compounds **7** and **8***

A mixture of hydrazine 2 (2.03 g, 1mmol) with different aldehydes; *P*-chloro benzaldehyde, *P*-nitro benzaldehyde (1mmol) was stirred at room temperature for 15 min. During stirring, the solid precipitate was formed, collected and filtered off, then dried and recrystallized with ethanol to be afforded.

4-(2-(4-chlorobenzylidene)hydrazinyl)-1-ethylquinolin-2(1*H*)-one (**7**)

Beige, yield (2.93 g, 90 %), m.p= 300-301 °C melts; IR (KBr, $cm^{-1}$): 3262 (NH), 3089 (C-$H_{aromatic}$), 2983 (C-$H_{aliphatic}$), 1630 (C=O), 1605 (C=N), 1562 (C=C), 1447 ($CH_{2bending}$), 1395 ($CH_{3bending}$), 1134 (C-C), 964, 883, 761. $^1$H NMR (DMSO-$d_6$): $\delta_H$ = 1.18 (t, 3H, *J*=4 $_{Hz}$, $CH_3$), 4.23 (q, 2H, *J*=4 $_{Hz}$, $CH_2$), 6.38 (s, 1H, 3-CH), 7.29 (t, 1H, *J*=12 $_{Hz}$, 7-$CH_{quinolinone}$), 7.52 (d, 2H, *o,o*-$CH_{benzene}$), 7.57 (d, 1H, *J*=8 $_{Hz}$, 8-$CH_{quinolinone}$),7.65 (t, 1H, *J* =8 $_{Hz}$, 6-$CH_{quinolinone}$), 7.79 (d, 2H, *m,m*-$CH_{benzene}$), 8.13 (d, 1H, *J*=8 $_{Hz}$, 5-$CH_{quinolinone}$), 8.37 (s, 1H, N=CH), 10.87 (s, 1H, $NH_{disappeared\ with\ D2O}$). $^{13}$C NMR (DMSO-$d_6$): $\delta_C$ = 162, 148, 143, 139, 134, 134, 132, 129, 129, 129, 129, 123, 121, 115, 114, 95, 36, 13. MS (70 eV) : *m/z* (%) = 328 (3.59) (M+2), 326 (M+) (38.97). Anal. Calcd for $C_{18}H_{16}ClN_3O$ (325.80) C 66.36; H 4.95; Cl 10.88; N 12.90. Found: C 66.29; H 4.93; Cl 10.85; N 12.89.

4-(2-(4-nitrobenzylidene)hydrazinyl)-1-ethylquinolin-2(1*H*)-one (**8**)

Orange, yield (3.19 g, 95 %), m.p= >300 °C; IR (KBr, $cm^{-1}$): 3296 (NH), 3113 (C-$H_{aromatic}$), 2989 (C-$H_{aliphatic}$), 1654 (C=O), 1600 (C=N), 1563 (C=C), 1447 ($CH_{2bending}$), 1393 ($CH_{3bending}$), 1130 (C-C), 907, 817, 747. $^1$H NMR (DMSO-$d_6$): $\delta_H$ = 1.19 (t, 3H, *J*=8 $_{Hz}$, $CH_3$), 4.24 (q, 2H, *J*=8 $_{Hz}$, $CH_2$), 6.47 (s, 1H, 3-CH), 7.30 (t, 1H, *J*=4 $_{Hz}$, 7-$CH_{quinolinone}$), 7.59 (d, 1H, *J*=12 $_{Hz}$, 8-$CH_{quinolinone}$), 7.66 (t, 1H, *J*=8 $_{Hz}$, 6-$CH_{quinolinone}$), 8.02 (d, 2H, *o,o*-$CH_{benzene}$), 8.15 (d, 1H, *J*=8 $_{Hz}$, 5-$CH_{quinolinone}$), 8.29 (d, 2H, *m,m*-$CH_{benzene}$), 8.47 (s, 1H, N=CH), 11.15 (s, 1H, $NH_{disappeared\ with\ D2O}$). MS (70 eV) : *m/z* (%) = 336 (M+) (27.05). Anal. Calcd for $C_{18}H_{16}N_4O_3$ (336.35) C 64.28; H 4.79; N 16.66. Found: C 64.26; H 4.75; N 16.65.

*2.2. Antitumor activity*

The antitumor activity of hydrazone compounds 3a-f was investigated against **HepG-2** cells (human Hepatocellular carcinoma) which were obtained from VACSERA Tissue Culture Unit. From Sigma (St. Louis, Mo., USA), DMSO, Crystal violet stain (1%) (It is composed of 0.5% (w/v) crystal violet and 50% methanol, then made up to volume with double distilled $H_2O$ and filtered through a Whatmann No.1 filter paper) and trypan blue dye were purchased. Moreover, from Lonza, Belgium, Fetal Bovine serum, Dulbecco's modified Eagle's medium (DMEM), 4-(2-hydroxyethyl)-1-piperazineethanesulfonic acid buffer solution (HEPES), L-glutamine, gentamycin and 0.25% Trypsin-EDTA were purchased. All cancer cell lines were maintained at 37ºC in a humidified atmosphere with 5% $CO_2$ in DMEM supplemented with 10% heat-inactivated fetal bovine serum, 1% L-glutamine, HEPES buffer and 50µg/ml gentamycin and subcultured two times a week.

For cytotoxicity assay, the cells were seeded in a 96-well plate at a cell concentration of $1\times10^4$ cells per well in 100µl of growth medium. After 24 h of seeding fresh medium including different concentrations of the test sample was added. Serial two-fold dilutions of the tested chemical compound were added to confluent cell monolayers distributed into 96-well, flat-bottomed microtiter plates (Falcon, NJ, USA) using a multichannel pipette. The microtiter plates were incubated at 37ºC for a period of 24 h in a humidified incubator with 5% $CO_2$. Three wells were used for each concentration of the test sample. Control cells were incubated without test sample and with or without DMSO. The little percentage of DMSO present in the wells (maximum 0.1%) was found not to affect the experiment. After incubation of the cells at 37°C, for 24 h, the viable cells yield was determined by a colorimetric method.

Briefly, after the end of the incubation period, media were aspirated, and the crystal violet solution (1%) was added to each well for at least 30 min. The stain was removed, and the plates were rinsed using tap water until all the excess stain was removed. Glacial acetic acid (30%) was then added to all wells and completely mixed, and then the absorbance of the plates was measured after being gently shaken on a Microplate reader (TECAN, Inc.), using a test wavelength of 490 nm. All results were edited for background absorbance revealed in wells without added stain. Treated samples

were compared with the cell control in the absence of the tested compounds. All experiments were proceeded in triplicate. The cell cytotoxic effect of each tested compound was calculated. The optical density was measured with the microplate reader (SunRise, TECAN, Inc, USA) to determine the number of viable cells and the percentage of viability was calculated as [the mean optical density of wells treated with the tested sample (ODt)/ the mean optical density of untreated cells (ODc)]x100%. The relationship between surviving cells and drug concentration is incurred to acquire the survival curve of each tumor cell line after treatment with the distinctive compound. The 50% inhibitory concentration (IC50), the concentration required to cause toxic effects in 50% of intact cells, was evaluated from graphic plots of the dose response curve for each conc. Using Graph pad Prism software (San Diego, CA. USA).

*2.3. Computational Details*

All quantum chemical computations were implemented by the Gaussian 09 program package [**40**] using Khon-Sham's density function theory (DFT) method subjected to the gradient-corrected hybrid density functional B3LYP method [**41**]. This function is a combination of the Becke's three parameters of non-local exchange potential with the non-local correlation functionality of Lee et al [**42,43**]. A full geometry optimization for each structure was performed using this function [**41**] and the 6-311++G (d, p) basis set [**44**]. No symmetry constrains were applied during the geometry optimization. Gaussian output files and all geometries were visualized either using GaussView 5.0.9 [**45**] or chemcraft 1.6 [**46**] software packages. DFT is applied to calculate $E_{HOMO}$, $E_{LUMO}$, $E_{gap}$. As well as additional chemical quantum parameters were also calculated such as: ionization potential ($I$), electron affinity ($A$), electronegativity ($\chi$), chemical potential (V), chemical hardness ($\eta$), global softness ($S$), electrophilicity (ω), nucleophilicity ($\varepsilon$) and additional electronic charge ($\Delta N$) according to the following equations [**47,48**]:

$$I = -E_{HOMO} \quad (1)$$

$$A = -E_{LUMO} \quad (2)$$

$$\chi = \frac{I+A}{2} \quad (3)$$

$$\eta = \frac{I-A}{2} \quad (4)$$

$$S = \frac{1}{2\eta} \quad (5)$$

$$\omega = \frac{\mu^2}{2\eta} \quad (6)$$

$$\varepsilon = \frac{1}{\omega} \quad (7)$$

$$V = -\chi \quad (8)$$

$$\Delta N = -\frac{V}{\eta} \quad (9)$$

Also, the total static dipole moment (μ), (Δα) and (β), values were computed using the following equations [**49,50**]:

$$\mu = (\mu^2 x + \mu^2 y + \mu^2 z)^{1/2},$$

$$\langle\alpha\rangle = 1/3\ (\alpha xx + \alpha yy + \alpha zz)$$

$$\Delta\alpha = ((\alpha xx - \alpha yy)^2 + (\alpha yy - \alpha zz)^2 + (\alpha zz - \alpha xx)^2/2)^{1/2}$$

$$\langle\beta\rangle = (\beta^2 x + \beta^2 y + \beta^2 z)^{1/2} \quad (10)$$

Where,

$$\beta x = \beta xxx + \beta xyy + \beta xzz,$$

$$\beta y = \beta yyy + \beta xxy + \beta yzz,$$

$$\beta z = \beta zzz + \beta xxz + \beta yyz. \quad (11)$$

For the conversion factors of $\alpha$, $\beta$, and HOMO and LUMO energies in atomic and CGS units: 1 atomic unit (a.u.) = $0.1482 \times 10^{-24}$ electrostatic unit (esu) for polarizability $\langle\alpha\rangle$; 1 a.u. = $8.6393\times10^{-33}$ esu for first hyperpolarizability $\langle\beta\rangle$; 1 a.u. = 27.2116 eV for HOMO and LUMO energies.

## 3. Results and Discussion

*3.1. Chemistry of the synthesized compounds*

The key intermediates, 4-hydrazino-1-ethylquinolin-2(1*H*)-one (**2**) were obtained *via* the reaction of 4-hydroxy-1-ethylquinolin-2(1*H*)-one (**1**) with a mixture of hydrazine and hydrazine dihydrochloride in dichlorobenzene according to the literature (Scheme 1) [23]. Treatment of hydrazinoquinolinone **2** with benzaldehyde was refluxed in absolute ethanol for 15min led to 4-(2-benzylidenehydrazinyl)-1-ethylquinolin-2(1*H*)-one (**3**) in 85% yield (Scheme 1). In the IR spectrum, it was observed that $NH_2$ peaks disappeared, and the NH group appeared at 3223 and the C=N group appeared at 1605 with comparison with hydrazino compound **2**. $^1$HNMR spectrum showed three specific singlet signals, at δ 6.39, 8.39 and 10.80 for the proton of 3-CH, N=CH and NH which was disappeared by $D_2O$, respectively. Also, the aromatic region revealed multiplet and doublet signals at δ 7.40 and 7.77 for benzene ring protons. In the $^{13}$CNMR spectrum, a special signal was displayed, in addition to new aromatic carbons, at δ 148 assigned as C=N group.

The molecular weight is consistent with the molecular formula of hydrazone compound **3** as shown in mass spectra and elemental analyses.

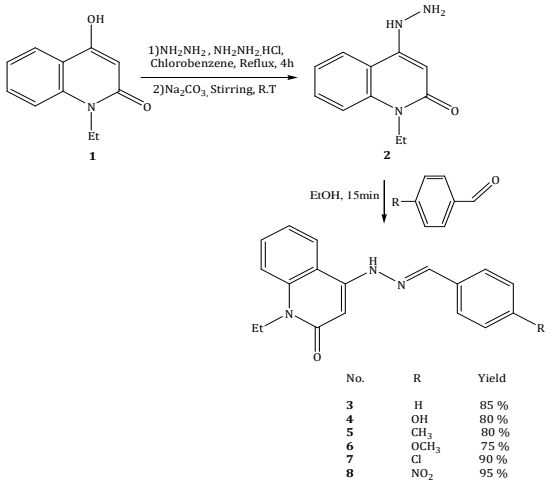


**Scheme 1:** Synthesis of hydrazone compounds 3-8 from hydrazinoquinolinone 2.

To study the effect of electron donating and electron withdrawing groups, we synthesized our target compounds to show their effect on hydrazono compound **3**. In the case of the donating group, the reaction of hydrazinoquinolinone **2** with *P*-hydroxyl benzaldehyde led to compound **4** with a yield of 80%. The IR spectrum showed a new characteristic broad band at 3300-2600 $cm^{-1}$ for the OH group.

The $^1$H-NMR spectrum of compound **4** exhibited chemical shifts due to two deuterium exchangeable protons at δ 10.58 and 9.90 for NH function and OH, respectively. The two singlet signals appeared at δ 6.33 and 8.30 for protons at positions 3 and N=CH, respectively. Also, the aromatic protons of benzene ring were represented at δ 7.60 for *o,o* positions but the protons of *m,m* positions exhibited a higher upfield shift at δ 6.86 as it became more shielded due to the presence of OH. Similarly, 4-(2-(4-methylbenzylidene) hydrazinyl)-1-ethylquinolin-2(1*H*)-one (**5**) was obtained *via* refluxing of hydrazinoquinolinone **2** and *P*-methylbenzaldehyde in 80% yield.

The $^1$H-NMR spectrum of compound **5** represented a specific singlet signal for $CH_3$ at δ 2.34, in addition to, three singlet signals at δ 6.37, 8.35 and 10.75 for protons at positions 3, N=CH and NH, respectively. In addition to the aromatic protons of the benzene ring which were observed higher upfield shifted at δ 7.63 for *o,o* positions and 7.27 for *m,m* positions because of the $CH_3$ group. Moreover, $^{13}$CNMR spectrum revealed a particular signal at δ 22 for $CH_3$. Also, condensation of hydrazinoquinolinone **2** with *P*-Anisaldehyde gave 4-(2-(4-methoxybenzylidene) hydrazinyl)-1-ethylquinolin-2(1*H*)-one (**6**) with a yield of 75%.

$^1$H-NMR spectrum of compound **6** presented a distinctive singlet signal at δ 3.81 for O-$CH_3$. As well, represented upfield shifted three singlet signals at δ 6.34, 8.33 and 10.66 for protons at positions 3, N=CH and NH, respectively. Furthermore, the aromatic protons of the benzene ring at δ 7.71 for *o,o* positions and 7.03 for *m,m* positions showed higher upfield shifted due to the neighboring O-$CH_3$ group, as it was a donating group so the electron density increased specially on *m,m* positions and became more shielded. The $^{13}$CNMR spectrum showed an exceptional signal at δ 56 for O-$CH_3$ group. The overcrowding of electron density on the groups by the strong electron donating groups OH, $OCH_3$ and $CH_3$ respectively, in compounds **4**, **5** and **6** exhibited a pronounced effect in their lower chemical shift relative to their parent compound **3**, such as protons at position 3, N=CH, NH and the aromatic protons of the benzene ring. While, in the case of the withdrawing group, 4-(2-(4-chlorobenzylidene)hydrazinyl)-1-ethylquinolin-2(1*H*)-one (**7**) was obtained *via* reacting hydrazinoquinolinone **2** with *P*-chlorobenzaldehyde at room temperature in 90% yield.

The $^1$H-NMR spectrum of compound **7** showed three singlet signals at higher chemical shifts 6.38, 8.37 and 10.87 for proton at position 3, N=CH and NH, respectively. As well, exhibited downfield shifted for protons of the benzene ring at δ 7.52 for *o,o* positions and 7.79 for *m,m* positions, precisely the protons in position *m,m* were strongly shielded than the protons of *o,o* positions due to the effect of Cl atom. The mass spectrum revealed molecular ion peak M+ at m/z 326 (38.97 %) along with M+2 at m/z 328 (3.59 %). Moreover, hydrazino quinolinone **2** with *P*-nitro benzaldehyde was stirred at room temperature for 15 min led to the formation of 4-(2-(4-nitrobenzylidene)hydrazinyl)-1-ethylquinolin-2(1*H*)-one (**8**) with 95 % yield.

The $^1$H-NMR spectrum of compound **8** revealed observable downfield shifting for all the protons which appeared strongly deshielded. The three singlet signals were represented at δ 6.47, 8.47 and 11.15 for protons at positions 3, N=CH and NH, respectively. Also, the aromatic protons of the benzene ring are presented at δ 8.02 for *o,o* positions and 8.29 for *m,m* positions. Upon the examination of the spectral data for all compounds, the resonance induced the electron withdrawing and donating effect arranged in the same order.

The capability of deshielding of position-3, N=CH and NH proton is $NO_2$ > Cl > H > OH > $OCH_3$ > $CH_3$. Finally, it has been observed that electron withdrawing groups in the aromatic ring of benzaldehyde enhance the reaction rate and reduce the reaction time.

*3.2. Vibration assignments of compounds 3-8*

By comparing of the calculated vibration frequencies at DFT/B3LYP/6-311++G (d,p) with the measured values (**c.f. Tables 1-3**) and the accompanying FT-IR spectra assignments of the investigated compounds **3-8** are shown in **Figs (S1-S6)**. Studying vibration spectra is one more method used to track changes in the researched compounds **3-8**. Because the equations were applied to the single molecule, there may be discrepancies between the computed and measured vibration frequencies (i.e., gaseous state). The following are some extensive ways to complete the assignment: For the studied compounds **3-8,** the computed vibration is designated as an N-H symmetric stretching vibration at 3199, 3192, 3206, and 3207 $cm^{-1}$, which has demonstrated a comparable agreement with experimental data at 3223, 3296, 3260, and 3278 $cm^{-1}$. In the range of 3000-3100 $cm^{-1}$, the aromatic C-H stretching vibrations [**51**] are typically detected. For the investigated compounds **3-8**, the computed vibration is attributed to C-H aromatic stretching vibrations at 3081, 3041, 3101, 3038, 3083, and 3102 $cm^{-1}$, which is equivalent to the experimental findings at 3082, 3046, 3099, 2968, 3089, and 3113 $cm^{-1}$. For the studied compounds **3-8**, the computed vibration, which is attributed to symmetric C-H aliphatic stretching vibration in $CH_3$ at 3001, 3001, 2991, 3001, 3001, and 3002 $cm^{-1}$, has demonstrated a comparable agreement with actual results at 2983, 2991, 2972, 2930, 2983, and 2989 $cm^{-1}$. Typically, the range between 1790 and 1810 $cm^{-1}$ is where the C=O vibrations [**51**] are found. For the studied compounds **3-8**, vibrations are attributed to C=O stretching at 1644, 1625, 1643, 1643, 1644, and 1665 $cm^{-1}$, respectively, which is compatible with experimental data at 1629, 1626, 1632, 1630, 1630, and 1654 $cm^{-1}$. For the analyzed compounds **3-8**, the computed vibration, which is asymmetric C=N Asym-stretching vibration at 1616, 1603, 1616, 1615, 1610, and 1599 $cm^{-1}$, has demonstrated comparable agreement with experimental data at 1605, 1600, 1601, 1605, 1605, and 1600 $cm^{-1}$. Typically, the region between 1480 and 1630 $cm^{-1}$ is where the C=C vibrations [**52**] are seen. For the studied compounds **3-8**, the calculated vibration is attributed to C=C stretching vibrations at 1580, 1580, 1584, 1580, 1580, and 1581 $cm^{-1}$, which is comparable to the results from the experiments at 1559, 1563, 1567, 1564, 1562, and 1563 $cm^{-1}$. For the investigated compounds **3-8**, the computed vibration is attributed to $CH_2$ bending vibrations at 1461, 1466, 1466, 1461, 1465, and 1466 $cm^{-1}$, which is comparable to the experimental findings at 1447, 1465, 1445, 1453, 1447, and 1447 $cm^{-1}$. As the same $CH_3$ bending vibrations at 1392, 1404, 1399, 1378, 1403, and 1393 $cm^{-1}$, which is comparable to the experimental findings at 1396, 1401, 1397, 1362, 1395, and 1393 $cm^{-1}$. For the studied compounds **3-8**, the calculated vibration is attributed to C-C stretching vibrations at 1119, 1118, 1135, 1130, 1127, and 1137 $cm^{-1}$, which is comparable to the results from the experiments at 1130, 1130, 1131, 1133, 1134, and 1130 $cm^{-1}$.

**Table 1:** Experimental and computational calculated vibrational wavenumbers (harmonic frequency ($cm^{-1}$)), (scaled and un-scaled values), IR intensities and assignments for compounds 3 and 4 at the B3LYP/6-311++G (d, p)

| | Compound 3 | | | | Compound 4 | | | |
|---|---|---|---|---|---|---|---|---|
| **Assignments** | **Exp.** | **Wave number** | | **IR Intensity** | **Exp.** | **Wave number** | | **IR Intensity** |
| | | **un-scaled** | **scaled** | | | **un-scaled** | **scaled** | |
| **υ $OH_{broad}$** | | | | | 3300-2600 | 3240-3032 | 3207-3001 | 1.22-30.94 |
| **υ NH** | 3223 | 3232 | 3199 | 1.99 | 3296 | 3225 | 3192 | 7.86 |
| **υ C-$H_{aromatic}$** | 3082 | 3113 | 3081 | 14.62 | 3046 | 3072 | 3041 | 25.98 |
| **υ C-$H_{aliphatic}$** | 2983 | 3032 | 3001 | 30.97 | 2991 | 3032 | 3001 | 30.94 |
| **υ C=O** | 1629 | 1661 | 1644 | 171.40 | 1626 | 1642 | 1625 | 614.10 |
| **υ C=N** | 1605 | 1633 | 1616 | 156.28 | 1600 | 1620 | 1603 | 35.49 |
| **υ C=C** | 1559 | 1596 | 1580 | 63.39 | 1563 | 1596 | 1580 | 57.00 |
| **β $CH_{2bending}$** | 1447 | 1476 | 1461 | 121.94 | 1465 | 1481 | 1466 | 101.46 |
| **β $CH_{3bending}$** | 1396 | 1407 | 1392 | 35.55 | 1401 | 1419 | 1404 | 42.06 |
| **υ C-C** | 1130 | 1131 | 1119 | 267.81 | 1130 | 1135 | 1118 | 196.78 |

**υ (Stretching); β (In plane bending).**

**Table 2:** Experimental and computational calculated vibrational wavenumbers (harmonic frequency ($cm^{-1}$)), (scaled and un-scaled values), IR intensities and assignments for compounds 5 and 6 at the B3LYP/6-311++G (d, p)

| | Compound 5 | | | | Compound 6 | | | |
|---|---|---|---|---|---|---|---|---|
| **Assignments** | **Exp.** | **Wave number** | | **IR Intensity** | **Exp.** | **Wave number** | | **IR Intensity** |
| | | **un-scaled** | **scaled** | | | **un-scaled** | **scaled** | |
| **υ NH** | 3260 | 3239 | 3206 | 1.50 | 3278 | 3240 | 3207 | 1.12 |
| **υ C-$H_{aromatic}$** | 3099 | 3133 | 3101 | 7.20 | 2968 | 3069 | 3038 | 27.56 |
| **υ C-$H_{aliphatic}$** | 2972 | 3022 | 2991 | 29.98 | 2930 | 3032 | 3001 | 31.14 |
| **υ O-C** | | | | | 2833 | 3011 | 2980 | 63.31 |
| **υ C=O** | 1632 | 1660 | 1643 | 160.66 | 1630 | 1660 | 1643 | 159.62 |
| **υ C=N** | 1601 | 1633 | 1616 | 164.64 | 1605 | 1632 | 1615 | 190.21 |
| **υ C=C** | 1567 | 1600 | 1584 | 9.00 | 1564 | 1596 | 1580 | 59.76 |
| **β $CH_{2bending}$** | 1445 | 1481 | 1466 | 104.16 | 1453 | 1476 | 1461 | 23.92 |
| **β $CH_{3bending}$** | 1397 | 1414 | 1399 | 42.00 | 1362 | 1392 | 1378 | 191.48 |
| **υ C-C** | 1131 | 1147 | 1135 | 22.20 | 1133 | 1142 | 1130 | 15.16 |

**υ (Stretching); β (In plane bending).**

**Table 3:** Experimental and computational calculated vibrational wavenumbers (harmonic frequency ($cm^{-1}$), (scaled and un-scaled values), IR intensities and assignments for compounds 7 and 8 at the B3LYP/6-311++G (d, p).

| | Compound 7 | | | | Compound 8 | | | |
|---|---|---|---|---|---|---|---|---|
| **Assignments** | **Exp.** | **Wave number** | | **IR Intensity** | **Exp.** | **Wave number** | | **IR Intensity** |
| | | **un-scaled** | **scaled** | | | **un-scaled** | **scaled** | |
| **υ NH** | 3262 | 3240 | 3207 | 1.59 | 3296 | 3239 | 3206 | 1.68 |
| **υ C-$H_{aromatic}$** | 3089 | 3115 | 3083 | 13.85 | 3113 | 3134 | 3102 | 6.68 |
| **υ C-$H_{aliphatic}$** | 2983 | 3032 | 3001 | 29.19 | 2989 | 3033 | 3002 | 28 |
| **υ C=O** | 1630 | 1644 | 1644 | 160.19 | 1654 | 1682 | 1665 | 29.75 |
| **υ C=N** | 1605 | 1627 | 1610 | 203.63 | 1600 | 1616 | 1599 | 3.16 |
| **υ C=C** | 1562 | 1596 | 1580 | 65.41 | 1563 | 1597 | 1581 | 69.95 |
| **β $CH_{2bending}$** | 1447 | 1480 | 1465 | 108.45 | 1447 | 1481 | 1466 | 111.54 |
| **β $CH_{3bending}$** | 1395 | 1418 | 1403 | 14.38 | 1393 | 1408 | 1393 | 32.87 |
| **υ C-C** | 1134 | 1139 | 1127 | 24.80 | 1130 | 1149 | 1137 | 157.89 |

**υ (Stretching); β (In plane bending).**

*3. 3. NMR analysis*

Utilizing TMS as a standard reference, the observed and anticipated $^{1}$H and $^{13}$C NMR chemical shifts of compounds **3-8** were acquired in DMSO solvent (**Figs. (S7-S17**) and **Tables (S18-S20)).** With relatively high correlation coefficients, the experimental chemical shifts are rather effectively reproduced (97–99.50 %). The hybrid B3LYP technique and GIAO were primarily used to complete the whole geometry optimization of the molecules at the gradient corrected DFT [**53**]. By comparing the discrepancies in $^{13}$C NMR chemical shift predictions with the observed results range from 1.51 to 18.00 ppm. The variance ranges for $^{1}$H NMR chemical shift predictions for experimental values are 1.17–11.15 ppm.

*3.4. Electronic structures*

*3.4. 1. Geometry structure*

Using density functional theory DFT/B3LYB at 6-311++G (d,p) basis set, all the studied compounds **3-8** have been investigated to determine various structural and chemical properties. **Fig. 1** and **Tables (S21-S22)** displayed the optimized geometrical parameters (bond lengths, bond angles and dihedral angles). According to DFT analysis, all the compounds **3-8** have a C1 point group symmetry.

The computed bond lengths for the studied compounds **3-8** in the chromone moiety range from 1.357 to 1.529 Å (c.f. **Tables S21-S22**). According to references [**54,55**] in the literature, they were overestimated by 1% compared to experimental values. Whereas the C=C bond lengths (1.385-1.397Å) did not significantly differ from the C=C bond length in ethylene [**54**], the C-C bond lengths for compounds **3-8** (1.409-1.457Å) were found to be like the central bond in butadiene (1.463Å) [**55**]. The significantly longer O-C bond lengths and shorter C=O bond lengths pointed to these results. The slight variation between calculated and observed bond lengths specified the power of the method used in the calculation, which was carried out in the gas phase and observed in solid-state. When compared to the experimental values, the calculated bond angles of the compounds show no significant change (c.f. **Tables S21-S22**). So, there is no planarity for all compounds as indicated by the dihedral angles (c.f. **Table S22**).

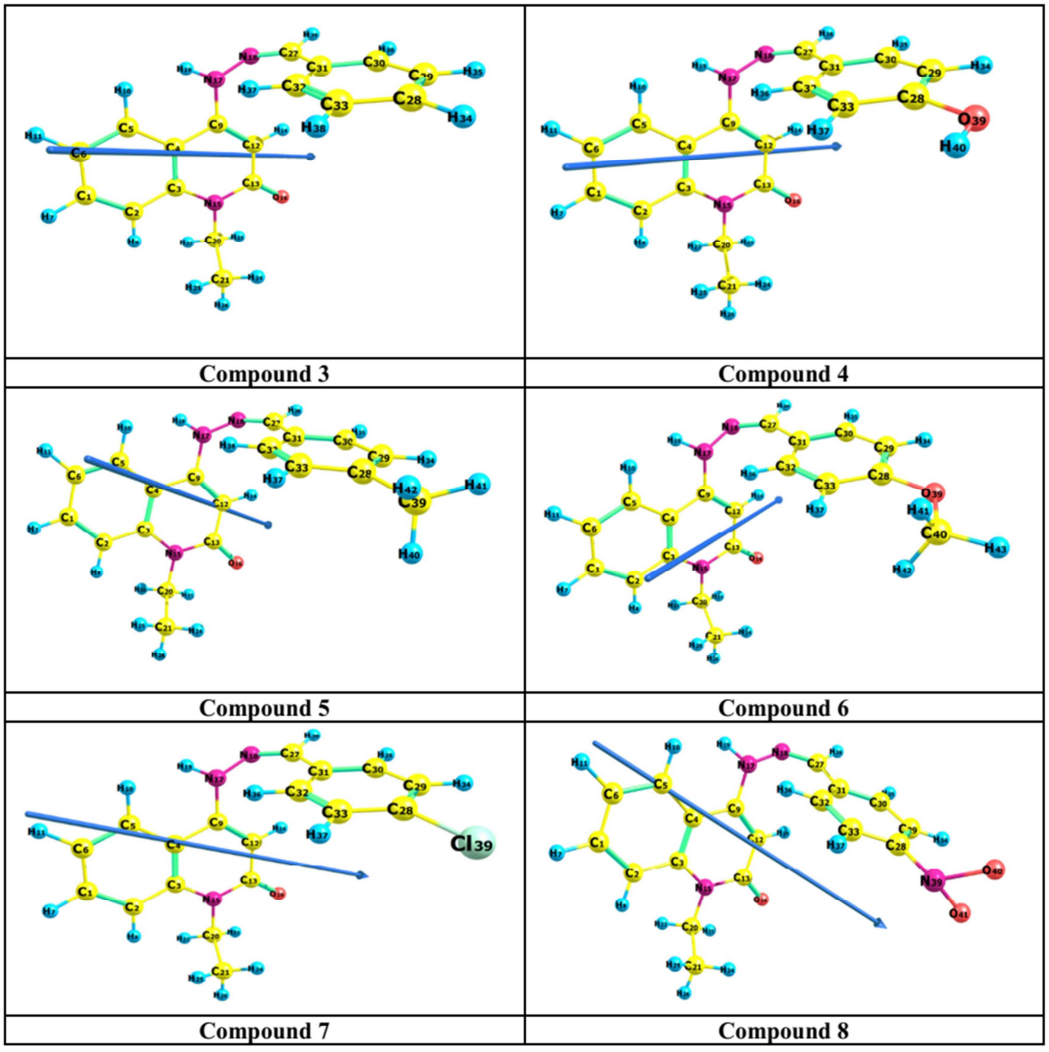


**Figure 1:** The optimized structure, perspective view of dipole moment of the studied compounds 3-8 at B3LYP/6-311++G (d, p)

*3.4.2. Frontier molecular orbital energies analysis*

The HOMO and LUMO Frontier molecular orbitals (FMOs), as well as their energy gap (ΔE gap), help characterize the chemical reactivity and kinetic molecular stability. FMOs and their quantum chemical characteristics are utilized to explain many types of reactions and identify the most sensitive regions through conjugated structures [**56**]. The HOMO serves as an illustration of the ability to contribute an electron, whereas the LUMO acts as an electron acceptor and denotes the ability to gain an electron. The charge disbursement and energy levels (**Fig. 2**) for the studied compounds **3–8**, at the HOMO→LUMO, orbitals were measured at B3LYP/6-311++G (d, p) level. The calculations showed that the charge distribution at the HOMO stage is primarily dependent on the charge of the Quinolinones moiety as well as the lone pairs of the N and O atoms. In contrast, the charge in LUMO vitality was distributed with an anti-bonding usefulness mostly throughout the hydrazone moiety and benzene ring. The FMO mechanism, which is visible in the electronic transition, has been used to confirm the intramolecular charge transfer. The studied compounds **3–8** had substantially smaller energy gaps (ΔE gap), which supported their softer character. Compound **8** (Egap = 3.702 eV) has the lowest energy gap during its HOMO→LUMO energy transition. It can be a softer molecule because the gap is smaller. As a result of their higher transitions, the volume of energy gaps continued to expand. The results in **Table 4** and **Fig. 2** suggest that the order of the calculated reactivity in the gas phase of the studied compounds is: **8** > **7** > **3** > **5** > **6** > **4**. This indicates that the smaller the $E_{gap}$, the higher the reactivity of these compounds. Finally, the theoretically calculated dipole moment, μ, which measures the charge separation over the molecule. The general trend of the dipole moment changes for the studied compounds follows the order **6** > **4** > **8** > **5** > **3** > **7** (**c.f. Table 4**) and the vector of the dipole moment is presented in **Figs. 1**

**Table 4:** Total energy, energy of HOMO and LUMO, energy gap, dipole moment, the ionization potential (I /eV), electron affinity (A /eV), chemical hardness ($\eta$ / eV), global softness (S/eV$^{-1}$), chemical potential ($V$/eV$^{-1}$), electronegativity ($\chi$/eV), global electrophilicity index, ($\omega$/eV), and additional electronic charge (ΔN/eV) of the studied compounds (3-8) computed at the$B_3$LYP/6-311++G (d, P)

| **Compounds** | **3** | **4** | **5** | **6** | **7** | **8** |
|---|---|---|---|---|---|---|
| **$E_T$ (au)** | -935.8581 | -1011.1075 | -975.1867 | -1050.4166 | -1395.4808 | -1140.2885 |
| **$E_{HOMO}$ (eV)** | -6.1075 | -6.0716 | -6.0580 | -6.0205 | -6.2049 | -6.3112 |
| **$E_{LUMO}$ (eV)** | -1.9579 | -1.8083 | -1.8610 | -1.7579 | -2.1338 | -2.6090 |
| **$E_{gap}$ (eV)** | 4.1496 | 4.2633 | 4.1970 | 4.2626 | 4.0711 | 3.7022 |
| **μ (Debye)** | 3.6833 | 4.8027 | 3.9245 | 5.0937 | 3.5885 | 4.7776 |
| ***I* (eV)** | 6.1075 | 6.0716 | 6.0580 | 6.0205 | 6.2049 | 6.3112 |
| ***A* (eV)** | 1.9579 | 1.8083 | 1.8610 | 1.7579 | 2.1338 | 2.6090 |
| ***X* (eV)** | 4.0327 | 3.9400 | 3.9595 | 3.8892 | 4.1694 | 4.4601 |
| ***V* (eV$^{-1}$)** | -4.0327 | -3.9400 | -3.9595 | -3.8892 | -4.1694 | -4.4601 |
| **$\eta$ (eV)** | 2.0748 | 2.1317 | 2.0985 | 2.1313 | 2.0356 | 1.8511 |
| ***S* (eV$^{-1}$)** | 0.2410 | 0.2346 | 0.2383 | 0.2346 | 0.2456 | 0.2701 |
| **$\omega$ (eV)** | 3.9191 | 3.6412 | 3.7354 | 3.5485 | 4.2700 | 5.3732 |
| **Δ *N* (eV)** | 1.9437 | 1.8483 | 1.8868 | 1.8248 | 2.0482 | 2.4094 |

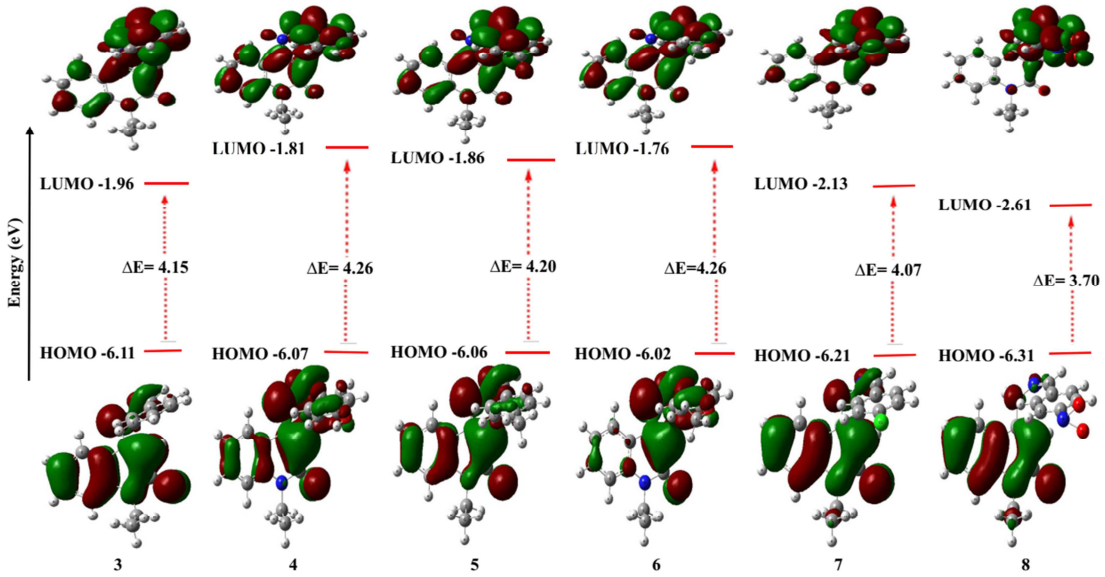


**Figure 2:** Energy of HOMO, LUMO and energy gap of the studied compounds 3-8 at B3LYP/6-311++ G (d, p) level of theory

*3.4.3. Global chemical reactivity descriptors*

To agree on qualitative chemical terms, the density functional theory (DFT) has actively contributed by offering theoretical background. Numerous anticipated and applied quantum chemical reactivity descriptors have been used to examine chemical reactivity and site specificity. The global chemical reactivity descriptors (GCRD), which provide information on molecular reactivity, are frequently employed to describe the general existence of molecules in connection to their chemical resistance. The small energy gaps for FMOs revealed the highly reactive character of the studied compounds **3–8**, towards their antimicrobial, antibacterial, and antifungal properties [**36-39**]. Based on B3LYP/6-311++G (d, p) level of theory, the global reactivity parameters $E_{HOMO}$, $E_{LUMO}$, $\Delta E_{gap}$, the electron affinity (*A*), electronegativity ($\chi$, eV), global softness (*S*, $eV^{-1}$), the ionization potential (*IP*), chemical hardness ($\eta$, eV), chemical potential (*V*, $eV^{-1}$), global electrophilicity index, ($\omega$, eV), and additional electronic charge ($\Delta N_{max}$) for the studied compounds **3–8**. The *IP* (ionization potential) and *EA* (electron affinity) are very significant characteristics as their evaluation helping in determination of the exact electronegativity ($\chi$, eV), and the exact hardness ($\eta$). Additionally, the HOMO and LUMO single-electron orbital energies are strongly related to these two variables. The studied compounds **3–8** were found to have ionization energies of 6.107 eV, 6.072 eV, 6.058 eV, 6.021 eV, 6.205 eV and 6.311 eV, respectively (**Table 4**). The compound **8** is the best donor of electrons because it had the lowest possible ionization value. The compound **6** is the best acceptor of electrons since it has the highest affinity value (1.758 eV). The molecular structure affects the chemical reactivity. As a result, compound **8** is found to be more active than compounds **3-7**. The negative chemical potential (V); indicates that the solid is difficult to maintain and won't decompose naturally into its parts. The range of values for the studied compounds **3–8** (– 3.889 to – 4.460 eV) justifies their solid existence and the capability to resist minor environmental changes. A molecule's resistance to changes in the electron distribution is measured by its hardness. The relationship between hardness and aromaticity is the same. Molecules must be as strong as possible because general strength (both absolute and relative) can be connected to the aromaticity of various non-substituted aromatic compounds. "Hardness" means resistance to the molecular orbital deformation of the chemical structure under slight disruptions found during the chemical cycle. The η of the material is additionally connected to aromaticity. Compound **4** has a higher absolute hardness, which is 2.1317 eV. With a global softness value of 0.2701 eV, compound **8** has the lowest global softness value out of all compounds **3-7**. The chemical potential *V* (eV) of an electron determines how easily it may be removed, and this is related to its electronegativity. The tendency of electrons to leave the electronic cloud is represented by the chemical potential (*V*, $eV^{-1}$). When the value of *V* increases, the ability of a molecule to lose an electron will increase. The $\eta$ also signifies the magnitude of the resistance of the electronic cloud to distortion when it is

overcome with electrons from the physical environment. The studied compounds **3-8**, according to the energy gap (ΔE gap) and reactivity characteristic values, have retained strong reactivity. A higher global electrophilicity (ω) value describes a good electrophile, and a lower value of ω denotes a good nucleophile. Our calculations indicate that compound **8** (ω = 5.3732 eV) has a higher value of ω and is hence more likely to receive electrons rapidly and be easily attacked by nucleophiles. Compound **6** (ω = 3.5485), on the other hand, has a lower electrophilicity, indicating that it is either a strong nucleophile or it can lose electrons.

*3.5. Nonlinear property analysis*

The association between the molecular structure and the NLO phenomena for the compounds **3–8**, was also theoretically computed using DFT/B3LYP/6-311++G (d, p) [**53**]. The mean first-order hyperpolarizability ⟨$\beta$⟩ (Octa pole moment), the mean polarizability (<α>) (Quadrupole moment), the total static dipole moment (μ), and the anisotropy of the polarizability (Δα), of the compounds **3-8** are all shown in **Table 5**. Compound **6** has a computed high dipole moment of 5.0937 D compared to compounds **3-5** and **7-8** at B3LYP/6-311++G (d,p). Additionally, the computed mean polarizability (<α>) for compound **8** is $37.15 \times 10^{-24}$ esu, which is two times higher than *p*-nitroaniline (PNA) molecule. **Table 5** shows the order of increasing $\alpha$ with respect to PNA molecule, with values of $\alpha$, $\beta$: compounds **3-7** are ~ 1.7 and 2 times higher than (PNA), respectively. In addition, the computed mean first-order hyperpolarizability ⟨$\beta$⟩, of the compound **8** is $108.90 \times 10^{-30}$ esu and compound **6** is $104.53 \times 10^{-30}$ esu i.e., higher than PNA molecule (**Table 5**), whereas compounds **3-5** and **7** are ~ 2, times higher than the reference, respectively. The measured value suggests that the studied compounds **3-8** may be a potentially useful NLO material. Since the investigated chemical lacked any experimental NLO data, the reference material was *p*-nitroaniline (PNA), one of the common NLO structures [**58-60**].

**Table 5:** Total static dipole moment (μ), the mean polarizability (<α>), the anisotropy of the polarizability (Δα), and the mean first-order hyperpolarizability (<β>), for the studied compounds (3-8) computed at B3LYP/6-311++G (d, P)

| Property | PNA | 3 | 4 | 5 | 6 | 7 | 8 |
|---|---|---|---|---|---|---|---|
| $\mu_x$, D | | 0.5993 | 0.9899 | -0.0087 | 0.1061 | 1.4826 | 3.3381 |
| $\mu_y$, D | | -1.9707 | -1.4510 | -0.8018 | 0.6693 | -1.6071 | -2.5445 |
| $\mu_z$, D | | 3.0535 | 4.4700 | 3.8417 | 5.0484 | 2.8454 | 2.2821 |
| **μ, D**ebye [a] | 2.44 | 3.6833 | 4.8027 | 3.9245 | 5.0937 | 3.5885 | 4.7776 |
| $\alpha_{XX}$, a.u. | | -107.4615 | -120.8418 | -112.1904 | -124.4055 | -126.5716 | -140.7278 |
| $\alpha_{XY}$, a.u. | | -4.8438 | 0.4805 | -3.7356 | -0.4629 | 6.3032 | 12.7919 |
| $\alpha_{YY}$, a.u. | | -133.6952 | -139.4140 | -138.2996 | -139.8341 | -143.8589 | -147.3191 |
| $\alpha_{ZZ}$, a.u. | | -132.5061 | -134.2451 | -140.8045 | -144.7323 | -147.8571 | -151.6782 |
| $\alpha_{YZ}$, a.u. | | 4.1316 | 5.3361 | 4.4978 | 6.7485 | 1.9656 | 1.1297 |
| $\alpha_{XZ}$, a.u. | | 2.5794 | 4.8984 | 4.7617 | 3.8918 | 13.2085 | 16.2707 |
| $\langle\alpha\rangle \times 10^{-24}$ esu [b] | | -124.5543 | -131.5003 | -130.4315 | -136.3240 | -139.4292 | -146.5750 |
| $\Delta\alpha \times 10^{-24}$ esu | 22 | 28.2840 | 20.8265 | 30.3964 | 22.8104 | 32.2200 | 37.1499 |
| **βxxx,**a.u. | | 1.7075 | 46.0381 | -11.0915 | 19.7414 | 27.4160 | 83.8808 |
| **βxxy**,a.u. | | 52.2909 | 21.6930 | 51.7387 | 44.2195 | 16.8873 | -14.5467 |
| **βxyy**,a.u. | | 22.1756 | 26.7817 | 20.6223 | -3.5355 | 25.5430 | 31.7244 |
| **βyyy**,a.u. | | -35.2709 | -6.8315 | -2.9333 | 43.6222 | 22.1325 | 28.9431 |
| **βxxz**,a.u. | | 3.4751 | -8.8355 | 4.0587 | 12.9308 | -24.9082 | -32.4856 |
| **βxyz**,a.u. | | -10.4007 | -13.8616 | -17.2204 | -38.0975 | -12.6831 | -5.7621 |
| **βyyz**,a.u. | | 28.2226 | 38.7321 | 33.8221 | 33.3964 | 23.0116 | 15.2525 |
| **βxzz**, a.u. | | -12.1090 | -36.2753 | -13.2320 | -31.7208 | -9.2435 | -10.4639 |
| **βyzz**, a.u. | | 5.9506 | 6.9893 | -8.2726 | -8.8625 | -18.5410 | -20.9203 |
| **βzzz**, a.u. | | 15.6447 | 48.5329 | 18.0309 | 45.0444 | 27.9946 | 24.6568 |
| $\langle\beta\rangle \times 10^{-30}$ esu [c] | 15.5 | 82.9374 | 86.7555 | 70.8835 | 104.5291 | 69.0179 | 108.8970 |

[a, b, c] **PNA results are taken from references [58-60].**

*3. 6. MEP analysis*

The electronic density is responsible for the electrostatic molecular potential (MEP), which is a very useful indication for electrophilic target sites, nucleophilic contacts, and hydrogen-bonding connections [**61**]. The reactive behavior of a molecule has also been described using the MEP surface designs, and negative domains can be thought of as potential electrophilic spots and positive sectors as nucleophilic centers. The nucleophilic cores over the molecules during the current study exhibited positive (blue) sectors, whereas the electrophilic sites over the molecules showed negative (red) sections. On the title portion of Quinolinones, the places demonstrating the negative electrostatic potential in the understudied molecules were found. The places with positive potential were those where hydrogen atoms were nearby. The current study **3-8** revealed that the analyzed chemicals' atoms of nitrogen have the greatest detrimental impacts (**Fig. 3**). According to the research, all the investigated compounds **3-8** have a significant positive electrostatic potential distributed throughout their skeleton, which suggests that they may be tightly connected to the microorganism being studied's negative molecular electrostatic potential. The biological behaviors of molecules with these MEPs will be readily explained by the quantum chemical requirements.

The diversified values of the MEP surface were mapped with different range of colors as follows: red for electron rich, (partially negative charge); blue for electron deficient, (partially positive charge); light blue for (slightly electron deficient region); yellow for (slightly electron rich region); green for neutral (zero potential) respectively. The potential increases in the order: red < orange < yellow < green < blue [**57**].

*3.7. MAC analysis*

Only after understanding the remaining uncertainty, Mullikan atomic charges (MAC) for molecules can be interpreted in various ways with a high degree of consistency to almost identical values [**62**]. Mullikan charges are a methodology to calculate partial atomic charges from measurements made using computational chemistry methods. They are derived from the research of the Mullikan charge analysis. The Mullikan graphs were created utilizing the DFT/B3LYP system and the 6-311++G (d, p) basis set to determine the Mullikan atomic charges of the investigated compounds **3-8**. (**Fig. S23-S28**).

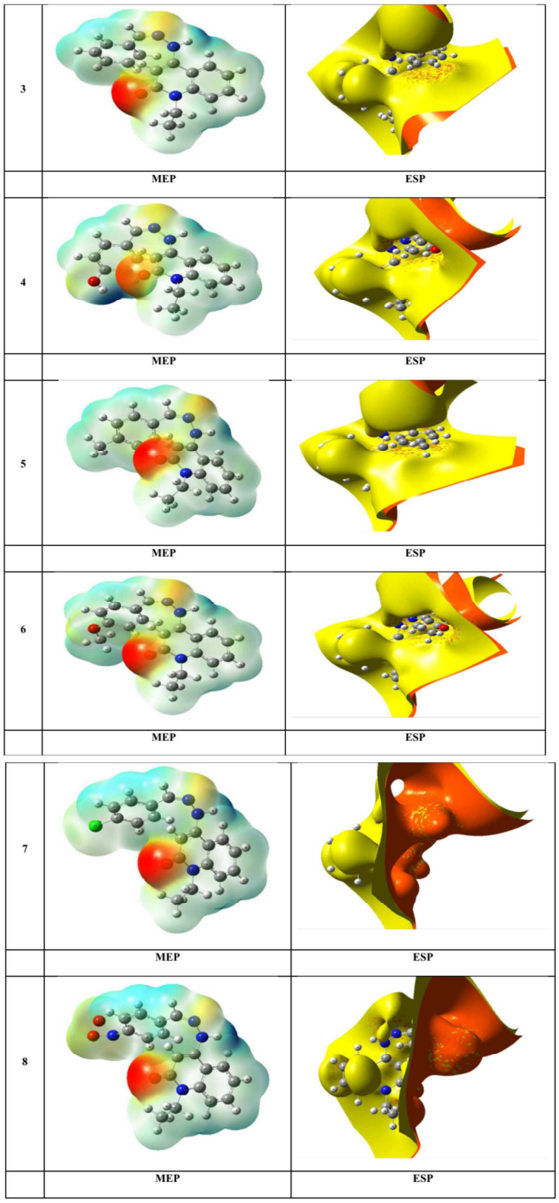


**Figure 3:** Molecular surfaces of the studied compounds 3-8 at B3LYP/6-311++G (d, p) level of theory

*3.8. Biological evaluation*

*Screening of antitumor activity of the synthesized compounds*

The antiproliferative activity of the novel synthesized compounds was evaluated in vitro against human tumor cell lines as hepatocellular carcinoma (HepG-2) for 24 h. Cisplatin was used as a reference drug, [**63-65**]. The

$IC_{50}$ technique, which measures the concentration of a scanned novel synthesized compounds in g/mL that inhibits proliferation (tumor cell growth) by 50% when compared to untreated control cells, was used to determine the growth inhibitory properties (**Table 6**). The survival curve for each type of cancer cell line after 24 hours was obtained by plotting the relationship between the surviving cells and the concentration of the tested chemicals as shown in **Fig. 4**. The results of IC50% values for the tested compounds revealed that compound **3** showed lower inhibited activity compared with cisplatin, whereas it exhibited the highest inhibitory activity against HepG-2 cells in comparison with the other tested compounds due to the difference in the nature of the substituent at the *para* position in the benzene ring in **Fig. 5**.

**Table 6:** Evaluation of cyclotoxicity against HepG-2 cell line for compounds 3-8

| Compound No. | $IC_{50}$ (µg/ml) |
|---|---|
| **3** | 29.82 ± 2.14 |
| **4** | 184.75 ± 8.65 |
| **5** | 311.72 ± 10.64 |
| **6** | 68.38 ± 4.06 |
| **7** | 426.76 ± 12.74 |
| **8** | 45.53 ± 3.29 |
| **cisplatin** | 3.67 ± 0.15 |

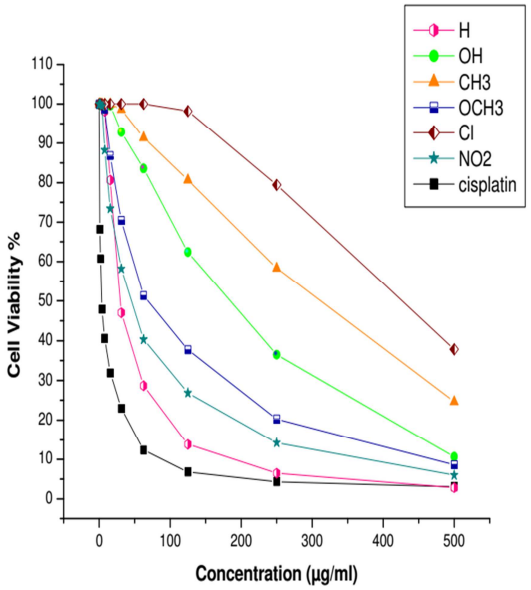


**Figure 4:** Effect of concentration (0-500 µg/ml) of the prepared compounds 3-8 and cisplatin as a standard drug on the proliferation of human liver cancer (HePG-2) cell line

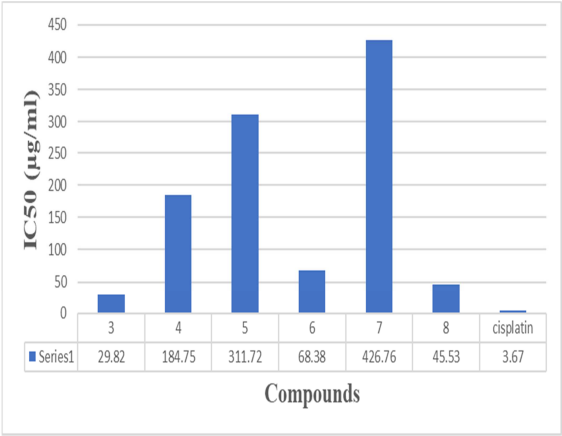


**Figure 5:** Virtual $IC_{50}$ values of the target compounds 3-8 against human liver cancer HepG-2 cell lines.

*Structure-activity relationship (SAR) analysis*

Structurally, it was found that further modifications were carried out in the benzene ring in compound **3** by substituting of hydrogen atom at *para* position to investigate the influence of the donating and withdrawing groups to study their effect on the antitumor activity. In the case of withdrawing groups, the behavior of both $NO_2$ and Cl groups was completely different against HepG-2 cells. It was observed that compound **8** exhibited the highest inhibitory activity relative to compound **7** and the other derivatives. While in the case of donating groups, compound **6** showed higher activity associated with inclusion of OCH3 with respect to other donating groups as shown in **Fig. 5**. Furthermore, compound **8** demonstrated higher antiproliferative activity than compound **6**. Briefly, the influence of the substituted groups on the antitumor inhibited activity was shown in the order: **8** > **6** > **4** > **5** > **7**.

## 4. Conclusion

In conclusion, a series of hydrazonoquinolinone derivatives **3**-**8** were successfully synthesized. From the treatment of hydrazinoquinolinone **2** with various substituted benzaldehyde bearing electron donating and withdrawing groups. The target compounds were identified using IR, $^{1}H$ NMR, $^{13}C$ NMR, mass spectra and elemental analysis. In NMR spectroscopic data, it was observed that the presence of withdrawing groups such as chloro and nitro groups in compounds **7** and **8**, respectively, showed a pronounced effect on chemical shift values for N=CH, 3-CH, the aromatic protons of the benzene ring and NH by increasing the electron donating group. All hydrazone compounds were investigated for *in vitro* cytotoxicity against HePG-2

(human liver cancer). From the results, most of the synthesized compounds afforded inhibitory action varying between low to high activity. Compound **3** was found to be the most active derivative in this series. By replacing of H in compound **3** with donating groups such as OH, $CH_3$ and $OCH_3$, it was found that compound **6** showed the highest inhibited activity with respect to the compounds containing donating groups, but lower than compound **3**. Moreover, in the case of withdrawing groups (Cl and $NO_2$), it was obvious that compound **8** displayed the highest antitumor activity with respect to the other hydrazone compounds but lower than compound **3**. Using (TD) DFT and the basis set B3LYP/6-311++G (d, p), a study was conducted to determine the reactive behavior of the investigated compounds **3-8**. The global reactivity descriptors are supported by the fact that the molecules are soft (because the energy gap is smaller), believed to be electrophilic (having a higher electrophilicity index), and more reactive (having a lower hardness). The chemical shift analysis from the NMR study indicated that the charges predicted by MEP were supported. Theoretically calculated vibrational wavenumbers were found to be in good agreement with experimental values.

## 5. Conflict of Interest

The authors declare that they have no known competing financial interests or personal relationships that could have appeared to influence the work reported in this paper.

## 6. Acknowledgements

Chemistry Department, Faculty of Education, Ain Shams University, Egypt, is greatly appreciated for supporting this research work.

## 7. References

[1] Ashraf A. Aly, Essmat M. El-Sheref, Momtaz E.M. Bakheet, Mai A.E. Mourad, Alan B. Brown, Stefan Bräse, Martin Nieger, Mahmoud A.A. Ibrahim, Synthesis of novel 1,2-bis-quinolinyl-1,4-naphthoquinones: ERK2 inhibition, cytotoxicity and molecular docking studies, Bioorganic Chemistry, 81, (2018), 700–712, https://doi.org/10.1016/j.bioorg.2018.09.017.

[2] Latchipatula Bhaskara Rao, Chinnabattigalla Sreenivasulu, Dakoju Ravi Kishore, Gedu Satyanarayana, Trending strategies for the synthesis of quinolinones and isoquinolinones, Tetrahedron, 127, (2022), 133093, https://doi.org/10.1016/j.tet.2022.133093.

[3] Deepak Bhasin, Somsundaram N. Chettiar, Jonathan P. Etter, May Mok, Pui-Kai Li, Anticancer activity and SAR studies of substituted 1,4-naphthoquinones, Bioorganic & Medicinal Chemistry, 21, (2013), 4662–4669, https://doi.org/10.1016/j.bmc.2013.05.017.

[4] Chung-Kyu Ryu, Dong-Hyun Kim, The synthesis, and antimicrobial activities of some 1,4-naphthoquinones, Arch. Pharm. Res., 15, (1992), 263–268, https://doi.org/10.1007/BF02974067.

[5] Yi-Lei Fan, Xiang-Wei Cheng, Jian-Bing Wu, Min Liu, Feng-Zhi Zhang, Zhi Xu, Lian-Shun Feng, Antiplasmodial and antimalarial activities of quinolone derivatives: an overview, European Journal of Medicinal Chemistry, 146, (2018), 1–14, https://doi.org/10.1016/j.ejmech.2018.01.039.

[6] Mohammed A.I. Elbastawesy, Ashraf A. Aly, Yaseen A.M.M. El-Shaier, Alan B. Brown, Gamal El-Din A. Abuo-Rahma, Mohamed Ramadan, New 4-thiazolidinone/quinoline-2-ones scaffold: Design, synthesis, docking studies and biological evaluation as potential urease inhibitors, Journal of Molecular Structure, 1244, (2021), 130845, https://doi.org/10.1016/j.molstruc.2021.130845.

[7] Yasuo Yamamoto, Mizuyo Kurazono, A new class of anti-MRSA and anti-VRE agents: Preparation and antibacterial activities of indole-containing compounds, Bioorganic & Medicinal Chemistry Letters, 17, (2007), 1626–1628, doi: 10.1016/j.bmcl.2006.12.081.

[8] Wafaa S. Hamama, Alaa E. Hassanien, Manal G. El-Fedawy, Hanafi H. Zoorob, Synthesis, PM3-Semiempirical, and Biological Evaluation of Pyrazolo[4,3-c] quinolinones, J. Heterocyclic Chem., 53, (2016), 945, doi: 10.1002/jhet.1747.

[9] Timothy M Rawson, Luke S P Moore, Nina Zhu, Nishanthy Ranganathan, Keira Skolimowska, Mark Gilchrist, Giovanni Satta, Graham Cooke, Alison Holmes, Bacterial and fungal co-infection in individuals with coronavirus: a rapid review to support COVID-19 antimicrobial prescribing, Clin. Infect. Dis. 71, (2020), 2459-2468, doi: 10.1093/cid/ciaa530.

[10] Arup K. Kabi, Raghuram Gujjarappa, Nagaraju Vodnala, Dhananjaya Kaldhi, Ujjawal Tyagi, Kalisadhan Mukherjee, Chandi C. Malakar, ―HFIP-mediated strategy towards β-oxo amides and subsequent Friedel-Craft type cyclization to 2-quinolinones using recyclable catalyst, Tetrahedron Lett., 61, (2020), 152535, doi: 10.1016/j.tetlet.2020.152535.

[11] EL-Shimaa Ibrahim, H. Moustafa, Shimaa Abdel Halim, Electronic Structure, Global Reactivity Descriptors and Nonlinear Optical Properties of Some Novel pyrazolyl quinolinone Derivatives. DFT approach, Egypt. J. Chem., 66, (2023), 375 – 385, doi: 10.21608/EJCHEM.2022.104957.4843.

[12] Mohammed A.I. Elbastawesy, Ashraf A. Aly, Mohamed Ramadan, Yaseen A.M.M. Elshaier, Bahaa G.M. Youssif, Alan B. Brown, Gamal El-Din A Abuo-Rahma, Novel Pyrazoloquinolin-2-ones: design, synthesis, docking studies, and biological evaluation as antiproliferative EGFR-TK inhibitors, Bioorg. Chem., 90, (2019), 103045, https://doi.org/10.1016/j.bioorg.2019.103045.

[13] Pavel Hradil, Petr Krejcˇí, Jan Hlavácˇ, Iveta Wiedermannová, Antonín Lycˇka, and Valerio Bertolasi, Synthesis, NMR spectra and X-ray data of chloro and dichloro derivatives of 3-hydroxy-2-phenylquinolin-4(1H)-ones and their cytostatic activity, Heterocycl. Chem., 41, (2004), 375.

[14] Simone Carradori and Romano Silvestri, New frontiers in selective human MAO-B inhibitors, Med. Chem, 58, (2015), 6717–6732, https://doi.org/10.1021/jm501690r
[15] Pescatori et al., L. ―N-Substituted Quinolinonyl Diketo Acid Derivatives as HIV Integrase Strand Transfer Inhibitors and Their Activity against RNase H Function of Reverse Transcriptase, J. Med. Chem., 58, (2015) ,4610–4623, doi: 10.1021/acs.jmedchem.5b00159.
[16] Hadida et al., S. ―Discovery of N -(2,4-Di- tert -butyl-5-hydroxyphenyl)-4-oxo-1,4-dihydroquinoline-3-carboxamide (VX-770, Ivacaftor), a potent and orally bioavailable CFTR potentiator, J. Med. Chem., 57, (2014), 9776–9795, doi: 10.1021/jm5012808.
[17] Xian-Qing Deng, Ming-Xia Song, Yan Zheng, Zhe-Shan Quan, Design, synthesis and evaluation of the antidepressant and anticonvulsant activities of triazole-containing quinolinones, Eur. J. Med. Chem., 73, (2014),217–224, doi: 10.1016/j.ejmech.2013.12.014.
[18] Pedro N. Batalha, Luana da S.M. Forezi, Nathalia M. de C. Tolentino, Fernanda S. Sagrillo, Vanessa G. de Oliveira, Maria Cecília B.V. de Souza and Fernanda da C.S. Boechat, 4-oxoquinoline derivatives as antivirals: a ten years overview, Current Top. Med. Chem. 20, (2020), 244–255, doi: 10.2174/1568026620666200129100219.
[19] Jin-Cherng Lien, Li-Jiau Huang, Che-Ming Teng, Jih-Pyang Wang, Sheng-Chu Kuo, Synthesis of 2-alkoxy 1,4-naphthoquinone derivatives as antiplatelet, anti-inflammatory, and antiallergic agents, Chem. Pharm. Bull., 50, (2002), 672–674, https://doi.org/10.1248/cpb.50.672.
[20] Yong-Ri Jin, Chung-Kyu Ryu, Chang-Kiu Moon, Mi-Ra Cho, Yeo-Pyo Yun, Inhibitory effects of J78, a newly synthesized 1,4-naphthoquinone derivative, on experimental thrombosis and platelet aggregation, Pharmacology, 70, (2004), 195–200, https://doi.org/10.1159/000075548.
[21] Dong Yeon Yuk, Changhwan Ryu, Jin-Tae Hong, Kwang-Hoe Chung, Won-Seek Kang, Y.I Kim, Hwan-Soo Yoo, Myung-Koo Lee, Chang-Ho Lee, Yang pu Yun, Antithrombotic and antiplatelet activities of 2-chloro-3-[4-(ehtylcarboxy)-phenyl]-amino-1,4-naphthoquinone (NQ12), a newly synthesized 1,4-naphthoquinone derivative, Biochem. Pharmacol., 60, (2000), 1001–1008, https://doi.org/10.1016/S00006-2952(00)00411-1.
[22] Tao Guo, Palladium/copper-catalyzed cross-coupling reactions for the synthesis of 4-heteroaryl quinolinone, Tetrahedron Letters, 57, (2016), 5837–5840, http://dx.doi.org/10.1016/j.tetlet.2016.11.056.
[23] Heba Hassan, Unanticipated Heterocyclization from Reaction of Hydrazine Hydrate and/or Hydrazine Dihydrochloride with 1-Ethyl-4-hydroxyquinolin-2(1H)-one, J. Heterocyclic Chem., 56, (2019), 646, doi: 10.1002/jhet.3443.
[24] Ya Wang, Shengxin Guo, Lijiao Yu, Wei Zhang, Zhenchao Wang, Yonggui Robin Chi , Jian Wu, Hydrazone derivatives in agrochemical discovery and development, Chinese Chemical Letters, (2023), https://doi.org/10.1016/j.cclet.2023.108207.
[25] Mustapha C. Mandewale, Udaysinha C. Patil, Supriya V. Shedge, Uttam R. Dappadwad, Ramesh S. Yamgar, A review on quinoline hydrazone derivatives as a new class of potent antitubercular and anticancer agents, Beni-Suef University Journal of Basic and Applied Sciences, 6, (2017), 354–361, http://dx.doi.org/10.1016/j.bjbas.2017.07.005.
[26] Sevim Rollas, Ş. Güniz Küçükgüzel, Biological Activities of Hydrazone Derivatives, Molecules, 12, (2007), 1910-1939, doi: 10.3390/12081910.
[27] Garima Verma, Akranth Marella, Mohammad Shaquiquzzaman, Mymoona Akhtar, Mohammad Rahmat Ali, Mohammad Mumtaz Alam, A review exploring biological activities of hydrazones, Journal of Pharmacy and Bioallied Sciences, 6, (2014), 69-80, https://doi.org/10.4103/0975-7406.129170.
[28] Sakineh Omidi, Ali Kakanejadifard, A review on biological activities of Schiff base, hydrazone, and oxime derivatives of curcumin, RSC Advances, 10, (2020), 30186–30202, https://doi.org/10.1039/D0RA05720G.
[29] Yıldız Uygun Cebeci, Özge Özşen Batur, Houssem Boulebd, New piperazine-hydrazone derivatives as potential antimicrobial agents: Synthesis, characterization, biological evaluation, and in silico investigations, Journal of Molecular Structure, 1289, (2023), 135791, https://doi.org/10.1016/j.molstruc.2023.135791.
[30] Łukasz Popiołek, The bioactivity of benzenesulfonyl hydrazones: A short review, Biomedicine & Pharmacotherapy, 141, (2021), 111851, https://doi.org/10.1016/j.biopha.2021.111851.
[31] Hamida Tlidjane, Nadjib Chafai, Salah Chafaa, Chawki Bensouici, Khalissa Benbouguerra, New thiophene-derived α-aminophosphonic acids: Synthesis under microwave irradiations, antioxidant, and antifungal activities, DFT investigations and SARS-CoV-2 main protease inhibition, J. Mol. Struct. 1250 (2022) 131853, https://doi.org/10.1016/j.molstruc.2021.131853.
[32] Noudjoud Houas, Salah Chafaa, Nadjib Chafai, Samira Ghedjati, Meriem Djenane, Siham Kitouni, Synthesis, characterization, DFT study and antioxidant activity of (2-hydroxynaphthalen-1- yl) methyl 2-hydroxyphenyl amino phosphonic acid, J. Mol. Struct. 1247 (2022) 131322, https://doi.org/10.1016/j.molstruc.2021.131322.
[33] Mouna Elkolli, Nadjib Chafai, Salah Chafaa, Imededdine Kadi, Chawki Bensouici, Abdelkader Hellal, New phosphinic and phosphonic acids: Synthesis, antidiabetic, anti-Alzheimer antioxidant activity, DFT study and SARS-CoV-2 inhibition, J. Mol. Struct. 1268 (2022) 133701, https://doi.org/10.1016/j.molstruc.2022.133701.
[34] Lilia Adjissi, Nadjib Chafai, Khalissa Benbouguerra, Imene Kirouani, Abdelkader Hellal, Houdheifa Layaida, Meriem Elkolli, Chawki Bensouici, Salah Chafaa, Synthesis, characterization, DFT, antioxidant, antibacterial, pharmacokinetics and inhibition of SARS-CoV-2 main protease of some heterocyclic hydrazones, J. Mol. Struct. 1270 (2022) 134005, https://doi.org/10.1016/j.molstruc.2022.134005.
[35] Juan J Villaverde, Carmen López-Goti, Manuel Alcamí, Al Mokhtar Lamsabhi, José L Alonso-Prados, Pilar Sandín-España, Quantum chemistry in

environmental pesticide risk assessment, Pest manag., 73 (2017) 2199-2202, doi: 10.1002/ps.4641.
[36] A. Elsamman, K.F. Khaled, Shimaa Abdel Halim, N.S. Abdelshafi, A critical view of the QSAR model for the prediction of a new bispyrazole derivative BPYR-P as a corrosion inhibitor for 304 SS in a 1.0 M HCl solution, Journal of Molecular Structure 1297 (2024) 136728, https://doi.org/10.1016/j.molstruc.2023.136728.
[37] Magdy A. Ibrahim, Al-Shimaa Badran, Shimaa Abdel Halim, N. Roushdy, A. A. M. Farag Enhanced structural and optical performance of the novel 3 [(5 amino 1 phenyl 1H pyrazol 4 yl) carbonyl] 1 ethyl 4 hydroxyquinolin 2(1H) one heterojunction: experimental and DFT modeling, Optical and Quantum Electronics 56 (2024) 257-292, doi:10.1007/s11082-023-05797-3.
[38] Mohamed A. Abdel-Rahman, Shimaa Abdel Halim Effects of solvents on structure and energy of 6-amino-2-mercapto-3H-- pyrimidin-4-one: A computational study, Journal of Molecular Liquids 395 (2024) 123821, doi:10.1016/j.molliq.2023.123821.
[39] Shimaa Abdel Halim, Ahmed M. El-Nahas & Asmaa B. El-Meligy, Safnaz H. El-Demerdash DFT study, and natural bond orbital (NBO) population analysis of 2 (2 Hydroxy phenyl) 1 azaazulene tautomers and their mercapto analouges, Scientific reports 14 (2024) 219, doi:10.1038/s41598-023-50660-w.
[40] Frisch M, J. G. W. Trucks, H. B. Schlegel, G, E. Scuseria, et al., Gaussian, Inc., Wallingford CT, (2009).
[41] Axel D. Becke, Density-functional thermochemistry, III: The role of exact exchange, J. Chem. Phys., 98, (1993), 5648-5652. doi: 10.1063/1.464913.
[42] Axel D. Becke, A new mixing of Hartree–Fock and local density-functional theories, J. Chem. Phys., 98, (1993), 1372-1376, doi: 10.1063/1.464304
[43] A. Jevicki, Choon-kyu Lee, S-matrix generating functional and effective action, 37, (1988), 1485–1491, doi: 10.1103/PhysRevD.37.1485.
[44] Stefanov B, B. G. Liu, A. Liashenko, P. Piskorz, I. Komaromi, R. L. Martin, D. J. Fox, T. Keith, M. A. Al-Laham, C. Y. Peng, A. Nanayakkara, M. Challacombe, P. M. W. Gill, B. Johnson, W. Chen, M. W. Wong, C. Gonzalez, J. A. Pople, Gaussian, Inc., Pittsburgh PA., (2003).
[45] GaussView, Version 5, Dennington, R.; Keith, T.; Millam, J. Semichem Inc., Shawnee Mission KS, (2009).
[46] http://www.chemcraftprog.com.
[47] N. Günay, H. Pir, Davut Avci, Yusuf Atalay, NLO and NBO analysis of sarcosine-maleic acid by using HF and B3LYP calculations, J. Chem., Article ID 712130 (2013), 1–16, doi: 10.1155/2013/712130.
[48] Ralph G. Pearson, Absolute electronegativity and hardness correlated with molecular orbital theory, Nati. Acad. Sci, 83, (1986), 8440–8441, doi: 10.1073/pnas.83.22.8440.
[49] Davut Avcı, Second and third-order nonlinear optical properties and molecular parameters of azo chromophores: semiempirical analysis, Spectrochim. Acta A., 82, (2011), 37-43, doi: 10.1016/j.saa.2011.06.037.
[50] Tomasz Seidler, Katarzyna Stadnicka, Benoît Champagne, Ab initio Hartree-Fock calculations on linear and second-order nonlinear optical properties of ionic organic crystals, J. Chem. Phys.,141, (2014), doi: 10.1063/1.4894483.
[51] Lambert J. B., H. F. Shurvell, L. Vereit, R. G. Cooks, G. H. Stout, Academic Press, New York, (1976).
[52] Kalsi P. S., Academic Press, New York, (2002).
[53] Kalinowski H. O., S. Berger, S. Braun, John Wiley &Sons, Chicheser, (1988).
[54] G. Mariappan, N. Sundaraganesan, FT-IR, FT-Raman, NMR spectra, density functional computations of the vibrational assignments (for monomer and dimer) and molecular geometry of anticancer drug 7-amino-2-methylchromone, J. Mol. Struct., 1063, (2014), 192–202, doi:10.1016/j.molstruc.2014.01.064.
[55] Mohamed G Kassem, Hazem A. Ghabbour, Hatem Abdel-Aziz, Hoong-Kun Fun, Chin Wei Ooi, 3-Chloro-4-methylquinolin-2(1H)-one, Acta Crystallogr. Sect. E, 68, (2012), 1043, doi:10.1107/S1600536812009889.
[56] Shimaa Abdel Halim, Huwaida M. E. Hassaneen, Experimental and theoretical study on the regioselective bis- or polyalkylation of 6-amino-2-mercapto-3*H*-pyrimidin-4-one using zeolite nano-gold catalyst and a quantum hybrid computational method, RSC. Adv. 12 (2022), 35794-35808, doi:10.1039/D2RA06572J.
[57] Natorajan, S.; Shanmugam G.; and Martin, S. A., Nonlinear Optical Properties of Organic Molecules and Crystals, Cryst Res Technal. 43, (2008), 561-569.
[58] Cheng, L. T.; Tam, W.; Stevenson, S. H.; Meredith, G. R.; Rikken, G.; Marder, S. R., Electric field induced second harmonic generation with and without fringes, J Phys Chem., 95, (1991), 10631-10640.
[59] Kaatz, P.; Donley, E. A.; Shelton, D. P. Analysis of nonlinear optical properties in donor–acceptor materials, J. Chem. Phys., 108, (1998), 849-858.
[60] T. Gnanasambandan, S. Gunasekaran, S. Seshadri, Experimental and theoretical study of p-nitroacetanilide. Spectrochimica. Acta Part A: Molecular and Biomolecular Spectroscopy, 117, (2014), 557-567, doi:10.1016/j.saa.2013.08.061.
[61] Zachary C. Holden, Bhaskar Rana, John M. Herbert, Analytic gradient for the QM/MM-Ewald method using charges derived from the electrostatic potential: theory, implementation, and application to ab initio molecular dynamics simulation of the aqueous electron, J Chem Phys, 150, (2019), 144115, doi:10.1063/1.5089673.
[62] Shimaa Abdel Halim, Tarik E. Ali, Somaia M. Abdel-Kariem Synthesis, DFT Calculations to investigate the Structure Electronic, Absorption Electronic Spectra, Antimicrobial Activity Application, and Non-Linear Optical Analysis of Pyridinyl and Pyrimidinyl Phosphonates, Iran. J.

Chem. Chem. Eng., 41,(2022), 1249-1274, doi: 10.30492/IJCCE.2021.523029.4523.

[63] Tim Mosmann, Rapid colorimetric assay for cellular growth and survival: application to proliferation and cytotoxicity assays. J. Immunol. Methods, 65, (1983), 55-63, doi:10.1016/0022-1759(83)90303-4..

[64] Sayed M. Riyadh, Sobhi M. Gomha, Elmahdi A. Mahmmoud, Mahmoud M. Elaasser, Synthesis and Anticancer Activities of Thiazoles, 1,3-Thiazines, and Thiazolidine Using Chitosan-Grafted-Poly(vinylpyridine) as Basic Catalyst, Heterocycles, 91, (2015), 1227-1243, doi:10.3987/COM-15-13210.

[65] Mahmoud F. Abo-Ashour, Wagdy M. Eldehna, Alessio Nocentini, Alessandro Bonardi, Silvia Bua, Hany S. Ibrahim, Mahmoud M. Elaasser, Vladimír Kryštof, Radek Jorda, Paola Gratteri, Sahar M. Abou-Seri, Claudiu T. Supuran, 3-Hydrazinoisatin-based benzenesulfonamides as novel carbonic anhydrase inhibitors endowed with anticancer activity: Synthesis, in vitro biological evaluation and in silico insights., Eur J Med Chem., 184, (2019), 111768, doi: 10.1016/j.ejmech.2019.111768.